Journal of Organometallic Chemistry 720 (2012) 73–80

Contents lists available at SciVerse ScienceDirect

Journal of Organometallic Chemistry

journal homepage: www.elsevier.com/locate/jorganchem

Square-planar mesitylenido(triphenylphosphane)nickel(II) complexes containing bidendate *N*,*O*-ligands: Changes in catalytic efficiency upon small alterations in the ligand backbone

Udo Beckmann [a,*,1], Monika M. Lindner [a,1], Eva Eichberger [a], Walter Frank [b]

[a] *Institut für Anorganische Chemie und Strukturchemie, Lehrstuhl I: Bioanorganische Chemie und Katalyse, Heinrich-Heine-Universität Düsseldorf, Universitätsstraße 1, 40225 Düsseldorf, Germany*

[b] *Institut für Anorganische Chemie und Strukturchemie, Lehrstuhl II: Material- und Strukturforschung, Heinrich-Heine-Universität Düsseldorf, Universitätsstraße 1, 40225 Düsseldorf, Germany*

ARTICLE INFO

Article history:
Received 21 June 2012
Received in revised form
14 August 2012
Accepted 27 August 2012

Keywords:
Nickel complexes
N,*O*-Ligands
Catalysis
Polyketone

ABSTRACT

Square planar arenido(triphenylphosphane)nickel(II) complexes containing a heterocyclic bidentate *N*,*O*-chelate ligand are catalysts for the copolymerisation of ethene and carbon monoxide. To examine the influence of the *N*,*O*-ligand on the catalytic activity new nickel(II) complexes with altered heterocyclic ring size in the corresponding *N*,*O*-ligands were synthesised and fully characterised. The crystal structures of all protonated *N*,*O*-ligands and the corresponding nickel complexes were determined. The catalytic activity of the new complexes in the copolymerisation reaction of ethene and carbon monoxide as well as in the polymerisation reaction of ethene were studied.

1. Introduction

Aliphatic polyketones produced by the catalysed copolymerisation of olefins and carbon monoxide are an interesting class of relatively new polymers. These thermoplastic copolymers exhibit outstanding characteristics such as chemical resistance and remarkable thermal properties [1–3]. Polyketones are featured by an exceptional environmental compatibility due to photodegradability through Norrish type I and II mechanisms [4–7], making them interesting materials in green chemistry. Industrially aliphatic polyketones are produced by the palladium catalysed copolymerisation of carbon monoxide and ethene yielding a strictly alternating aliphatic polyketone [8–11]. However, the costly noble metal palladium is not recovered and remains in the polymer. In the search for alternatives, nickel complexes turned out to be promising candidates. The most efficient nickel complex to date for the copolymerisation of ethene and CO, $\mathbf{K^{1'}}$, is shown in Fig. 1 [12].

It is already structurally characterised and contains a bidentate *N*,*O*-chelating ligand which coordinates to the nickel centre in a square planar manner forming a six-membered chelate ring. We were interested in tuning the catalytic activity of the complex by slightly altering the framework of the *N*,*O*-ligand. Kläui et al. showed that a prolonged perfluorinated alkyl chain (see Fig. 1) results in higher catalytic efficiencies whereas methyl or phenyl groups at the same position result in less efficient complexes and a methoxy group drops the efficiency to about zero [12]. In this work we report on altering the ring size of the heterocyclic ligand from five to six and seven membered rings, the synthesis and characterisation of the resulting nickel complexes and the studies of the new compounds as catalysts for the copolymerisation of ethene and CO.

2. Results and discussion

Complexes of the type shown in Fig. 1 can be prepared according to Scheme 1.

The reaction of the square-planar nickel complex (*SP*-4-3)-[NiBr(mes)(PPh_3)$_2$] (R = CH_3) or (*SP*-4-3)-[NiBr(2-tol)(PPh_3)$_2$] (R = H) with an appropriate deprotonated *N*,*O*-ligand $(\mathbf{L^{1-3}})^-$ yields the target complexes $\mathbf{K^{1-3}}$ and $\mathbf{K^{1'-3'}}$. We reported the syntheses of the ligands $\mathbf{HL^{1-3}}$ in a recent paper [13].

Complex $\mathbf{K^1}$ was synthesised as previously described [14]. The synthesis of $\mathbf{K^2}$ and $\mathbf{K^3}$ involves the deprotonation of the protonated *N*,*O*-ligand $\mathbf{HL^2}$ or $\mathbf{HL^3}$ and the following reaction of the

* Corresponding author. Fax: +49 211 81 12287.
E-mail address: Udo.Beckmann@uni-duesseldorf.de (U. Beckmann).
[1] U. Beckmann and M. M. Lindner contributed equally to this work.

0022-328X/$ – see front matter © 2012 Elsevier B.V. All rights reserved.
http://dx.doi.org/10.1016/j.jorganchem.2012.08.030

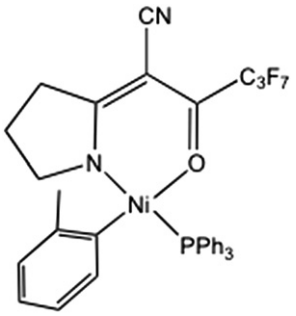

Fig. 1. The most efficient nickel complex $\mathbf{K^{1'}}$ for the copolymerisation of ethene and CO to date.

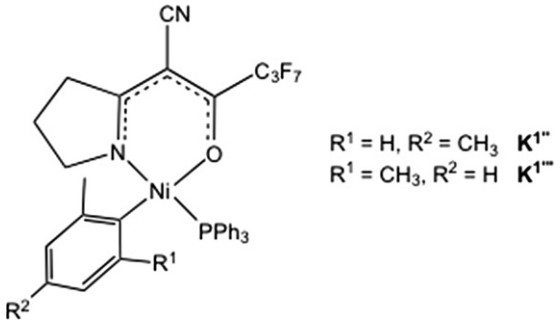

Fig. 2. Complexes with a xylenido ligand.

deprotonated ligand $(\mathbf{L^2})^-$ or $(\mathbf{L^3})^-$, respectively, with (*SP*-4-3)-[NiBr(mes)(PPh_3)$_2$] in a toluene solution. We investigated the suitability of several bases for the ligand deprotonation. No reaction takes place using e.g. triethylamine or "proton sponge" (1,8-bis(dimethylamino)naphthalene). Interestingly, triethylamine is a suitable base for the deprotonation of H$\mathbf{L^1}$, whereas with H$\mathbf{L^2}$ or H$\mathbf{L^3}$ no reaction occurs under equal conditions. We also tried to react the ligands H$\mathbf{L^{1–3}}$ with (SP-4-3)-[NiBr(mes)(PPh_3)$_2$] in the presence of silver(I) oxide which acts as base and bromide scavenger in heterogeneous phase. This again was only successful in the case of H$\mathbf{L^1}$, whereas H$\mathbf{L^2}$ and H$\mathbf{L^3}$ showed no reaction. Best results were achieved by first using sodium bis(trimethylsilyl)amide to generate the sodium salt of any of the three ligands in toluene solution and successively adding the sodium salt to a toluene solution of (*SP*-4-3)-[NiBr(mes)(PPh_3)$_2$].

Complex $\mathbf{K^1}$ is very similar to the already known and structurally characterised complex $\mathbf{K^{1'}}$ shown in Fig. 1 [12]. $\mathbf{K^1}$ comprises a mesitylenido ligand instead of a 2-toluenido ligand in $\mathbf{K^{1'}}$. We introduced the mesitylenido group mostly for stability reasons as the mesitylenido nickel(II) complexes turned out to be significantly more stable in benzene or dichloromethane solution in air than their 2-toluenido analogues. No decomposition that would be noticeable in the $^{31}P\{^1H\}$ NMR spectrum takes place in a benzene solution for weeks even under aerobic conditions, whereas the corresponding 2-toluenido nickel(II) complexes decompose to paramagnetic nickel(II) compounds, triphenylphosphane and triphenylphosphane oxide within days [15]. Decomposition is even faster in analogous complexes comprising a benzenido ligand. Closer examination showed that these complexes are only stable for a few hours in solution under inert conditions. The stability of the complex is obviously dependent on the number of methyl groups at the arenido ligand.

To distinguish the steric and inductive effects of the methyl groups at the arenido ligand we also synthesised the 2,4-xylenido and the 2,6-xylenido complexes $\mathbf{K^{1''}}$ and $\mathbf{K^{1'''}}$ (s. Fig. 2) in the same way as depicted in Scheme 1 except that (*SP*-4-3)-[NiBr(2,4-xyl)(PPh_3)$_2$] and (*SP*-4-3)-[NiBr(2,6-xyl)(PPh_3)$_2$] were used.

If the stabilising effect is mainly due to the sterical situation in the 2,6-position, the 2-toluenido complex $\mathbf{K^{1'}}$ and the 2,4-xylenido complex $\mathbf{K^{1''}}$ should have similar reactivities as well as the reactivities of the mesitylenido complex $\mathbf{K^1}$ and the 2,6-xylenido complex $\mathbf{K^{1'''}}$ should resemble. The stability and reactivity of the complexes were investigated using the previously described reaction with 2-hexyne [15]. 2-Hexyne inserts into the nickel–carbon bond and the resulting insertion product reacts under β-hydride elimination [15]. The four complexes $\mathbf{K^1}$, $\mathbf{K^{1'}}$, $\mathbf{K^{1''}}$ and $\mathbf{K^{1'''}}$ can be ranked qualitatively in the following order of decreasing reactivity: $\mathbf{K^{1'}} > \mathbf{K^{1''}} > \mathbf{K^{1'''}} > \mathbf{K^1}$, obviously due to the inductive effects of the methyl groups, not merely steric effects.

In solid state all complexes $\mathbf{K^{1–3}}$ and $\mathbf{K^{1'–3'}}$ appear to be air-stable, they form yellow to orange–red coloured crystals and were fully characterised.

The complexes $\mathbf{K^1}$ and $\mathbf{K^{1'}}$ are active catalysts in the homogeneous copolymerisation of carbon monoxide and ethene. We determined the overall efficiency (g polyketone per g Ni) of the catalyst complexes $\mathbf{K^{1–3}}$ in toluene solution (*ca.* 2–3 mM) at 60 °C and 50 bar (CO partial pressure: 10 bar, C_2H_4 partial pressure: 40 bar) in a standard 100 mL stainless steel autoclave setup comprising a glass inlet over 24 h. We found the efficiency of $\mathbf{K^1}$ varying between 8000 and 10,000, comparable to the previously reported efficiency for $\mathbf{K^{1'}}$ of about 11,000 [12], leading to polymers with molecular weights of $>10^5$ [16]. Interesting results were obtained using $\mathbf{K^2}$ and $\mathbf{K^3}$ as well as $\mathbf{K^{2'}}$ and $\mathbf{K^{3'}}$, respectively, in the same setup instead of $\mathbf{K^1}$. No formation of polyketone was observed.

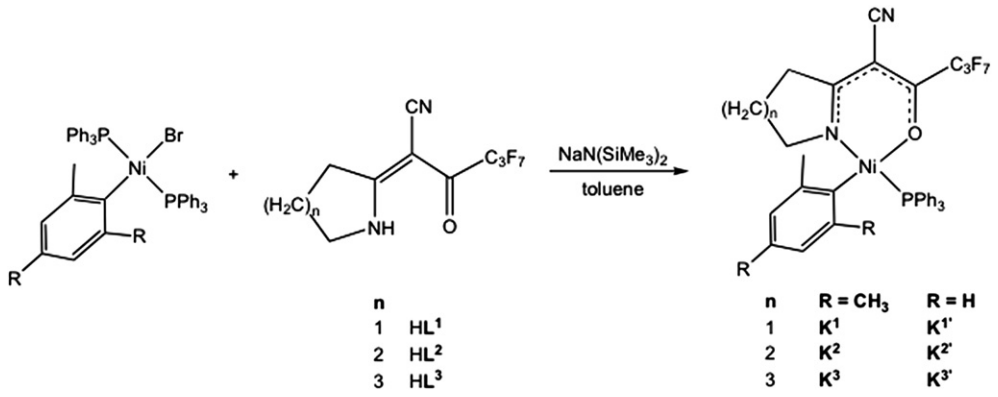

Scheme 1. Synthesis of the complexes $\mathbf{K^{1–3}}$ and $\mathbf{K^{1'–3'}}$.

The overall efficiency under the said conditions for **K²** and **K³** is zero. Even at higher temperatures up to 100 °C and up to 100 bar as well as varying the CO/ethene ratio no copolymerisation reaction takes place using **K²**, **K²′**, **K³** or **K³′** as catalysts.

In search for explanations for this unexpected behaviour in the copolymerisation of carbon monoxide and ethene, we investigated the reaction of the complexes **K¹′⁻²′** and **K¹⁻²** only with ethene and the catalytic activity for the polymerisation to polyethylene.

Complex **K¹′** is an active catalyst for the polymerisation of ethene yielding polyethylene [15]. In a standard 100 mL autoclave setup we used the respective complex in a *ca.* 10–15 mM solution in dry toluene. We added *ca.* 70 bar ethene and stirred at room temperature for 72 h. During that time, all of the ethene was consumed and reacted to polyethylene [15]. The same reaction procedure was applied to the other catalysts, **K¹**, **K²** and **K²′**. However, none of them yielded polyethylene. GC/MS analysis of the solutions after the catalysis experiments showed oligomers of ethene, ranging from the ethene dimer butene (C_4H_8) up to several isomers of hexadecene ($C_{16}H_{32}$), clearly identifiable by their fragmentation pattern in the EI mass spectra. Other reaction products detected by GC/MS analysis are 2-methylstyrene and isomers of 1-butenyl-2-methylbenzene in the case of the 2-toluenido complexes (**K¹′** and **K²′**) or 2,4,6-trimethylstyrene, isomers of 1-butenyl-2,4,6-trimethylbenzene and even small amounts of isomers of 1-(hexenyl)-2,4,6-trimethylbenzene in the case of the mesitylenido complexes (**K¹** and **K²**). From the existence of different oligomers with either hydrogen or the arenido ligand as end group can be concluded that ethene does not only insert into the nickel–carbon bond of the initial complex but also into the nickel–hydrogen bond of the nickel hydride complex that is formed after β-hydride elimination of the insertion product. We confirmed β-hydride elimination as the beginning of the decomposition reaction and thus as the start of the termination of the oligomerisation reaction by means of investigating the reaction of the complexes **K¹** and **K¹′** with olefins and alkynes as recently published [15].

To sustain a constant insertion of ethene into the nickel–carbon bond (or the nickel–hydrogen bond) a certain pressure of ethene is needed. As long as the pressure of ethene is high enough the insertion rate is higher than the β-hydride elimination rate and oligomers of ethene are formed. When the insertion rate decreases during the progress of the reaction a competition of ethene insertion and β-hydride elimination starts. The β-hydride elimination rate increases and eventually the insertion of ethene and thus the formation of oligomers or even polymers is terminated as the nickel–hydride complex reacts on towards paramagnetic decomposition products [15].

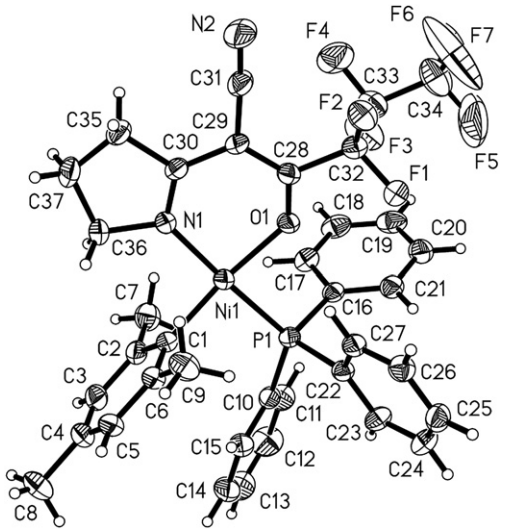

Fig. 4. Perspective view of complex **K¹**. Displacement ellipsoids are drawn at the 30% probability level.

While complex **K¹′** catalyses both the copolymerisation of ethene and carbon monoxide as well as the polymerisation of ethene, complex **K¹** is only active for the copolymerisation reaction and merely forms oligomers in the reaction with ethene. Complexes **K²** and **K²′** are neither active in the copolymerisation nor in the polymerisation. The ability for inserting ethene conforms to the reactivity for the insertion of carbon monoxide. **K¹′** easily inserts carbon monoxide at atmospheric pressure whereas the insertion of CO into the Ni–C bond of **K¹** only takes place in a 5 bar carbon monoxide atmosphere. This is reflected in the reactivity of the two complexes towards ethene. While **K¹′** polymerises ethene to yield polyethylene, **K¹** only produces ethene oligomers.

These observations lead us to the profound examination of both the protonated ligand molecules H**L¹⁻³** as well as the complexes **K¹⁻³**. We determined the crystal structure of all six compounds (Figs. 3–6).

Considering the data of Table 1 there are no obvious trends in bond lengths and angles in the solid state that follow the observed trend in catalytic activity. Again, no trend can be followed regarding

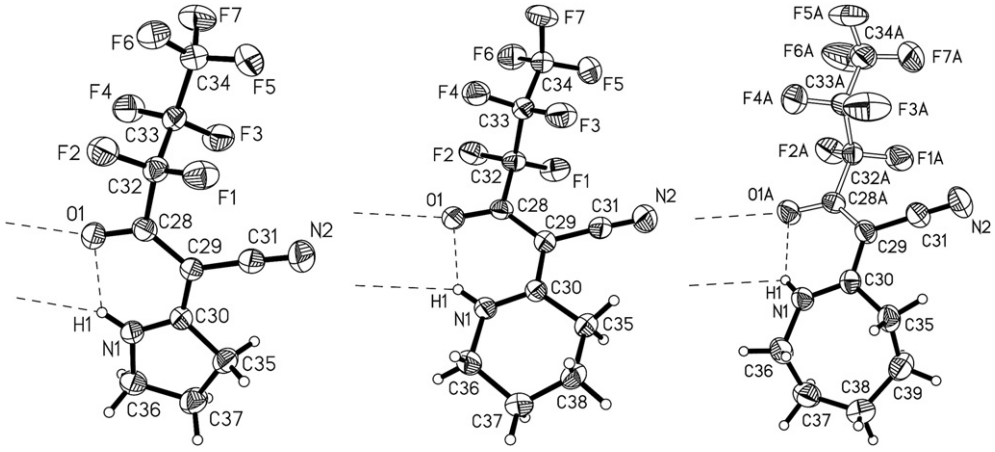

Fig. 3. Perspective view of H**L¹**, H**L²** and H**L³**. Displacement ellipsoids are drawn at the 30% probability level. Dashed lines indicate the directions of hydrogen bonding. The C_3F_7 group of H**L³** is disordered over two positions with only one of them being shown.

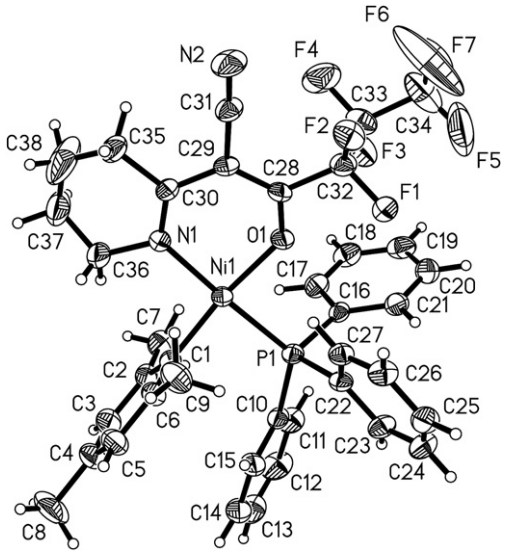

Fig. 5. Perspective view of complex **K²**. Displacement ellipsoids are drawn at the 30% probability level.

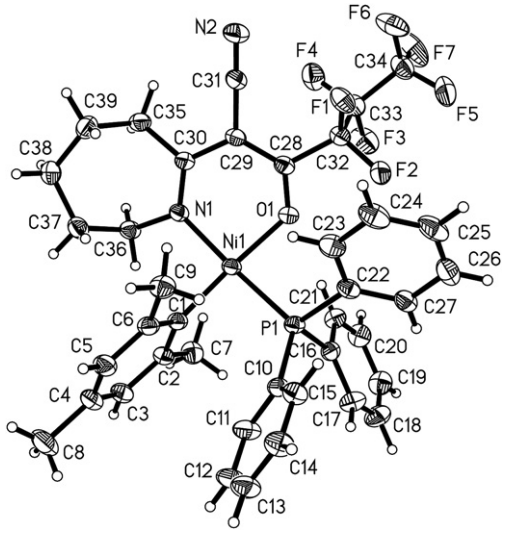

Fig. 6. Perspective view of complex **K³**. Displacement ellipsoids are drawn at the 30% probability level.

the ν(C≡N) stretching frequency in the IR spectra of the protonated and coordinated ligands (see Table 1).

Both the protonated ligands and the nickel complexes contain a delocalised π-system for which two resonance structures are relevant as depicted in Scheme 2. The contribution of the resonance structures in the ligands and the complexes is different with structure ***A*** seemingly being predominant in the ligands and structure ***B*** contributing more to the complexes. Apart from that the length of the N1–C30 bond does not change when considering the 3σ-criterion.

The only trend in the series **K¹⁻³** is observed in the intersection angle of the corresponding N–O–P–C mean plane with the ligand's N–C–C(CN)–C–O mean plane (Table 2, last row). With increasing ring size (n = 1–3) the intersection angle becomes larger as well, describing the non-coplanarity of the ligand framework with the square-planar coordination plane.

The increasing intersection angle could suggest that the *N,O*-ligand in the case of **K²** and **K³** takes on conformations in solution which make the approach and the coordination of a monomer difficult and might hinder the insertion into the nickel–carbon bond thus preventing the formation of polymer. Mechanistically the coordination of a monomer can follow either an associative or a dissociative pathway. In the associative case the monomer coordinates to the axial position of the square-planar nickel complex forming a square-pyramidal intermediate with the coordination number 5 which then rearranges via Berry pseudo-rotation to a trigonal-bipyramidal species that allows the insertion of the monomer into the nickel–carbon bond from a position *cis* to the arenido ligand. In the dissociative case one of the coordinated ligands, here presumably triphenylphosphane, would dissociate so that a species with a trifold coordination and a vacant coordination site for the monomer is formed. As previous experiments with triphenylphosphane added to the catalysis experiment showed [16] free PPh_3 has no influence on the catalytic activity thus indicating an associative pathway which is also suggested by the *trans*-effect of the triphenylphosphane ligand and the nitrogen atom of the *N,O*-chelating ligand. Furthermore the addition of Lewis acids such as triphenylborane and $B(C_6F_5)_3$ which can act as phosphane scavengers show no difference in long-term catalytic runs as previously described [16].

Dissociation of triphenylphosphane therefore is not necessary to enable catalytic activity and the difficulties in the polymerisation can be more likely attributed to a hindrance in monomer coordination and insertion. In contrary the dissociation of the triphenylphosphane ligand rather leads to decomposition of the catalyst complex.

In the case of a hindered approach and insertion of the monomers in solution the insertion rate of ethene will be lower and either no insertion at all takes place or – insertion presumed –

Table 1
Comparison of bond lengths (Å) and angles (°) in the protonated ligands H**L¹⁻³** with the corresponding data in the complexes **K¹⁻³** (see Figs. 3–6). For the disordered parts of **K³** mean values are given. IR ν(C≡N) stretching frequency (cm^{-1}, KBr disk) in H**L¹⁻³**, **K¹⁻³** and **K¹′⁻³′**. Data for H**L¹⁻³** see Ref. [13].

	H**L¹**	H**L²**	H**L³**	**K¹**	**K²**	**K³**	**K¹′** [12]	**K²′**	**K³′**
N1–C30	1.303(2)	1.299(3)	1.308(4)	1.290(4)	1.300(4)	1.301(3)	1.299(3)	–	–
C30–C29	1.405(3)	1.424(3)	1.429(4)	1.421(4)	1.435(5)	1.448(3)	1.438(4)	–	–
C29–C28	1.413(3)	1.428(3)	1.434(6)	1.368(4)	1.383(5)	1.376(3)	1.387(3)	–	–
C28–O1	1.231(2)	1.228(3)	1.232(6)	1.252(3)	1.266(4)	1.260(3)	1.267(3)	–	–
C29–C31	1.414(3)	1.426(4)	1.427(5)	1.436(4)	1.438(5)	1.430(3)	1.443(4)	–	–
C31–N2	1.141(2)	1.145(3)	1.133(4)	1.124(4)	1.131(4)	1.137(3)	1.135(5)	–	–
O1···X[a]	2.06(2)	2.02(3)	1.98(5)	1.915(2)	1.904(2)	1.9206(16)	1.918(2)	–	–
N1···X[a]	0.86(2)	0.84(3)	0.81(4)	1.903(3)	1.947(3)	1.9460(19)	1.926(2)	–	–
N1···O1	2.685(2)	2.673(2)	2.65(2)	2.735(4)	2.763(5)	2.715(4)	2.744(3)	–	–
N1···X···O1[a,b]	128.6(19)	133(3)	139(4)	91.51(9)	91.86(11)	89.17(7)	91.1(1)	–	–
ν(C≡N)	2213	2206	2209	2217	2211	2206	2216	2208	2226

[a] X = H1 or Ni1.
[b] "bite angle".

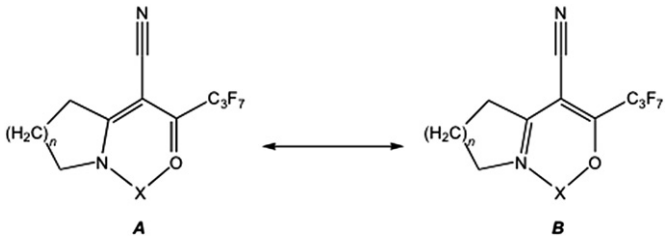

Scheme 2. The two resonance structures contributing to both the ligands H$\mathbf{L^{1-3}}$ and the complexes $\mathbf{K^{1-3}}$ with ***A*** contributing more to the ligands and ***B*** contributing more to the complexes.

Table 2
Comparison of bond lengths (Å) and angles (°) of complexes $\mathbf{K^{1-3}}$ and $\mathbf{K^{1'}}$.

	$\mathbf{K^{1'}}$ [12]	$\mathbf{K^{1}}$	$\mathbf{K^{2}}$	$\mathbf{K^{3}}$
Ni–P	2.1935(10)	2.1854(9)	2.1958(10)	2.1828(7)
Ni–C	1.893(2)	1.884(3)	1.886(4)	1.892(2)
Ni raised out of the N–O–P–C mean plane	0.03	0.03	0.04	0.03
Intersection angle of the C–Ni–P plane with the N–Ni–O plane	2.5	8.0	7.2	3.7
Intersection angle of the mesitylenido mean plane with the N–O–P–C mean plane	88.5	83.3	83.2	88.8
Intersection angle of the N–O–P–C mean plane with the ligand N–C–C(CN)–C–O mean plane	0.9	12.4	21.2	37.5

eventually β-hydride elimination will take over leading to the decomposition of the catalyst. Evidence for no insertion of the monomers is found in the gas chromatogram of the solution after the catalysis experiment of $\mathbf{K^2}$ with ethene. Mesitylene, the *N*,*O*-ligand H$\mathbf{L^2}$ and triphenylphosphane are detected. The appearance of these compounds in the gas chromatogram is due to the decomposition of the intact catalyst complex on the GC column. The decomposition of the complexes has been separately investigated by measuring a gas chromatogram of a freshly prepared toluene solution of $\mathbf{K^1}$ which showed the single components mesitylene, the *N*,*O*-ligand H$\mathbf{L^1}$ and triphenylphosphane as decomposition products. The protonation of the mesitylenido ligand and the *N*,*O*-ligand results from protonation by the slightly acidic column.

Comparison of the complexes $\mathbf{K^{1'}}$ and $\mathbf{K^1}$ also suggests a steric hindrance effect of the two ortho methyl groups at the mesitylenido ligand ($\mathbf{K^1}$) compared to the 2-toluenido analogue ($\mathbf{K^{1'}}$) with respect to monomer insertion.

Theoretical calculations are underway to better understand the described effects.

3. Conclusions

The nickel complexes $\mathbf{K^1}$ and $\mathbf{K^{1'}}$ comprising a *N*,*O*-chelate ligand with a five-membered heterocycle are catalysts for the copolymerisation of ethene and carbon monoxide [12,14]. We reported new nickel complexes in which the five-membered heterocycle of the bidentate *N*,*O*-ligand was altered to six- and seven-membered rings, $\mathbf{K^2}$, $\mathbf{K^{2'}}$, $\mathbf{K^3}$ and $\mathbf{K^{3'}}$. All four were tested as catalysts for the copolymerisation reaction of ethene and carbon monoxide, but unexpectedly none of them showed catalytic activity for the polymerisation reaction. Catalysis experiments with ethene yielded oligomers and products containing the arenido ligand and several ethene units whereas $\mathbf{K^{1'}}$ was found to polymerise ethene to polyethylene [15]. Reasons for this behaviour can be assumed in a decreasing insertion rate of ethene during the reaction, while β-hydride elimination takes over eventually leading to the decomposition of the catalyst [15]. The crystal structures of the complexes were determined in the search for information on a molecular basis. With an increasing heterocyclic ring size the intersection angle between the ligand framework and the square-planar coordination plane increases as well. This finding in solid state might be an approach to further understand the different catalytic behaviour. In solution this seems to lead to conformations that hinder the approach and coordination of monomers.

4. Experimental section

All reactions were carried out under nitrogen atmosphere using standard Schlenk techniques unless stated otherwise. All solvents were purified and degassed by standard procedures. Chemicals were bought from commercial sources like Acros, Sigma–Aldrich, Merck and Fluorochem. One-dimensional NMR spectra were recorded at room temperature, ^{1}H and ^{31}P{^{1}H} NMR spectra were recorded on a Bruker Avance DRX 200 spectrometer, and ^{13}C and ^{19}F NMR spectra were recorded on a Bruker Avance DRX 500 spectrometer. The proton chemical shifts are given in ppm and referenced to the signal of TMS or the solvent residual signal [17] (CD_2Cl_2: ^{1}H 5.30 ppm, C_6D_6: ^{1}H 7.16 ppm, ^{13}C 128.1 ppm, $CDCl_3$: 7.26 ppm). The fluorine chemical shifts are referenced to C_6F_6 (^{19}F −162.9 ppm) [18], the phosphorous chemical shifts are referenced to the signal of external H_3PO_4 (85%). The coupling constants are reported as their absolute value. Infrared spectra were recorded on a FT-IR Bruker IFS 66 spectrometer. Elemental analyses were performed on a Perkin–Elmer CHN-2400/II elemental analyser. GC/MS spectra were determined on a Thermo Finnigan Trace GC-Ultra Trace DSQ comprising a column of 15 m length with 0.25 mm in diameter and a DB5MS phase. Injection temperature was 220 °C, column temperature increased starting at 50 up to 250 °C with 20 °C min^{-1}. % Area is listed as intensity of the signal in the gas chromatogram. (*SP*-4-3)-[NiBr(2-tol)(PPh_3)$_2$] and (*SP*-4-3)-[NiBr(mes)(PPh_3)$_2$] were prepared according to modified literature procedures [14,19–21]. The preparation of the protonated ligands H$\mathbf{L^{1-3}}$ was reported previously [13]. Single crystals of H$\mathbf{L^{1-3}}$ suitable for X-ray diffraction were obtained by slow evaporation of a saturated diethyl ether solution of each ligand H$\mathbf{L^{1-3}}$. The synthesis of (*SP*-4-3)-[Ni($\mathbf{L^1}$)(2-tol)(PPh_3)] $\mathbf{K^{1'}}$ was carried out as described previously [14].

4.1. (SP-4-3)-[Ni($\mathbf{L^1}$)(mes)(PPh_3)] ($\mathbf{K^1}$)

The synthesis was carried out as previously described [14]. Single crystals of the complex suitable for X-ray diffraction were obtained upon cooling by slow crystallisation from hot methanol.

4.2. (SP-4-3)-[Ni($\mathbf{L^2}$)(mes)(PPh_3)] ($\mathbf{K^2}$)

382 mg (1.2 mmol) of 4,4,5,5,6,6,6-heptafluoro-3-oxo-2-piperidin-(2Z)-ylidene-hexanenitrile (H$\mathbf{L^2}$) were dissolved in 50 mL toluene. 2.0 mL (1.2 mmol) of sodium bis(trimethylsilyl) amide (0.6 M in toluene) was added and the mixture was stirred for 2 h. A solution of 939 mg (1.2 mmol) of (*SP*-4-3)-[NiBr(mes)(PPh_3)$_2$] [14] in 50 mL toluene was added dropwise with stirring. After complete addition stirring was continued overnight and the reaction mixture was filtered over celite®. The solvent was removed *in vacuo* and to the residue was added 20 mL pentane. After stirring overnight, the yellow precipitate was filtered, washed with pentane and dried *in vacuo* yielding 572 mg (63%) of $\mathbf{K^2}$. Single crystals suitable for X-ray diffraction were obtained by slow diffusion of

a pentane/hexane mixture (1:1) into a concentrated solution of **K²** in toluene. ^{1}H NMR (500.13 MHz, CD_2Cl_2, r.t., ppm): δ = 1.25 (X of [ABMX]$_2$, 2H, CH_2); 1.57 (M of [ABMX]$_2$, 2H, CH_2); 2.02 (s, 3H, *p*-CH_3); 2.61 (B of [ABMX]$_2$, 2H, CH_2); 2.65 (A of [ABMX]$_2$, 2H, CH_2); 2.78 (s, 6H, *o*-CH_3); 6.12 (s, 2H, mes); 7.20 (C of [A[BC]$_2$], 6H, PPh_3); 7.28 (B of [A[BC]$_2$], 6H, PPh_3); 7.35 (A of [A[BC]$_2$], 3H, PPh_3). ^{31}P{^{1}H} NMR (202.46 MHz, CD_2Cl_2, r.t., ppm): δ = 24.0. ^{19}F NMR (470.54 MHz, CD_2Cl_2, r.t., ppm): δ = −81.6 (t, $^4J_{FF}$ = 9.4 Hz, CF_3); −115.2 (q, $^4J_{FF}$ = 9.4 Hz, $COCF_2$); −126.5 (s, CF_2−CF_3). IR (KBr disk, cm^{-1}): $\tilde{\nu}$ = 3053 (m, C−H$_{aromat.}$); 2940 (m, C−H$_{aliphat.}$); 2211 (vs, C≡N); 1590 (vs, C=O); 1576 (vs, C=C); 1435 (m, P−C); 1228 (s, C−F). $C_{38}H_{34}N_2OF_7PNi$ (757.35): calcd. C 60.26, H 4.52, N 3.70; found C 59.9, H 4.7, N 3.9.

4.3. (SP-4-3)-[Ni(**L²**)(2-tol)(PPh$_3$)] (**K²′**)

The synthesis was carried out as for **K²**, except that 902 mg (1.2 mmol) of (*SP*-4-3)-[NiBr(2-tol)(PPh$_3$)$_2$] was used. Yield: 430 mg (49%) of **K²′**. Single crystals suitable for X-ray diffraction were obtained by slow diffusion of a pentane/hexane mixture (1:1) into a concentrated solution of **K²′** in toluene. ^{1}H NMR (500.13 MHz, CD_2Cl_2, r.t., ppm): δ = 1.26 (X of [ABMX]$_2$, 2H, CH_2); 1.57 (M of [ABMX]$_2$, 2H, CH_2); 2.63 (A of [ABMX]$_2$, B of [ABMX]$_2$, *o*-CH_3, 7H); 6.33 (m, 1H, *o*-tol); 6.45 (m, 1H, *o*-tol); 6.53 (m, 1H, *o*-tol); 7.24–7.39 (m, 16H, PPh_3 + *o*-tol). ^{31}P{^{1}H} NMR (202.46 MHz, CD_2Cl_2, r.t., ppm): δ = 27.2. ^{19}F NMR (470.55 MHz, CD_2Cl_2, r.t., ppm): −81.6 (t, $^4J_{FF}$ = 7 Hz, 3F, CF_3); −115.0, −115.8 (dq, $^2J_{FF}$ = 273 Hz, $^4J_{FF}$ = 9 Hz, 2F, C(O)CF_2); −126.2, −126.8 (d, $^2J_{FF}$ = 286 Hz, 2F, CF_2−CF_3). IR (KBr disk, cm^{-1}): $\tilde{\nu}$ = 3053 (m, C−H$_{aromat.}$); 2941 (m, C−H$_{aliphat.}$); 2208 (vs, C≡N); 1590 (vs, C=O); 1577 (vs, C=C); 1435 (m, P−C); 1229 (s, C−F). $C_{36}H_{30}N_2OF_7PNi$ (729.30): calcd. C 59.29, H 4.15, N 3.84; found C 59.2, H 3.9, N 3.9.

4.4. (SP-4-3)-[Ni(**L³**)(mes)(PPh$_3$)] (**K³**)

The synthesis was carried out as for **K²**, except that 399 mg (1.2 mmol) of 2-azepan-(2Z)-ylidene-4,4,5,5,6,6,6-heptafluoro-3-oxo-hexanenitrile (H**L³**) was used. Yield: 722 mg (78%). Single crystals suitable for X-ray diffraction were obtained by slow diffusion of a pentane/hexane mixture (1:1) into a concentrated solution of **K³** in toluene. ^{1}H NMR (500.13 MHz, CD_2Cl_2, r.t., ppm): δ = 0.97 (X of [ADMNX]$_2$, 2H, CH_2); 1.53 (M and N of [ADMNX]$_2$, 4H, $(CH_2)_2$); 2.01 (s, 3H, *p*-CH_3); 2.79 (s, 6H, *o*-CH_3); 2.92 (D of [ADMNX]$_2$, 2H, CH_2); 3.08 (A of [ADMNX]$_2$, 2H, CH_2); 6.12 (s, 2H, mes); 7.21 (C of [A[BC]$_2$], 6H, PPh_3); 7.28 (B of [A[BC]$_2$], 6H, PPh_3); 7.36 (A of [A[BC]$_2$], 3H, PPh_3). ^{31}P{^{1}H} NMR (202.46 MHz, CD_2Cl_2, r.t., ppm): δ = 23.6. ^{19}F NMR (470.54 MHz, CD_2Cl_2, r.t., ppm): δ = −81.7 (t, $^4J_{FF}$ = 9.4 Hz, CF_3); −115.1 (q, $^4J_{FF}$ = 9.4 Hz, $COCF_2$); −126.8 (s, CF_2−CF_3). IR (KBr disk, cm^{-1}): $\tilde{\nu}$ = 3023 (m, C−H$_{aromat.}$); 2935 (m, C−H$_{aliphat.}$); 2206 (vs, C≡N); 1585 (vs, C=O); 1506 (vs, C=C); 1437 (m, P−C); 1228 (s, C−F). $C_{39}H_{36}N_2OF_7PNi$ (771.38): calcd. C 60.73, H 4.70, N 3.63; found C 61.0, H 4.8, N 3.5.

4.5. (SP-4-3)-[Ni(**L³**)(2-tol)(PPh$_3$)] (**K³′**)

The synthesis was carried out as for **K²**, except that 902 mg (1.2 mmol) of (*SP*-4-3)-[NiBr(2-tol)(PPh$_3$)$_2$] and 399 mg (1.2 mmol) of 2-azepan-(2Z)-ylidene-4,4,5,5,6,6,6-heptafluoro-3-oxo-hexanenitrile (H**L³**) were used. Yield: 410 mg (46%) of **K³′**. Single crystals suitable for X-ray diffraction were obtained by slow diffusion of a pentane/hexane mixture (1:1) into a concentrated solution of **K³′** in toluene. ^{1}H NMR (500.13 MHz, CD_2Cl_2, r.t., ppm): δ = 0.96 (X of [ADMNX]$_2$, 2H, CH_2); 1.53 (M and N of [ADMNX]$_2$, 4H, $(CH_2)_2$); 2.60 (s, 3H, *o*-CH_3); 2.90 (D of [ADMNX]$_2$, 2H, CH_2); 3.05 (A of [ADMNX]$_2$, 2H, CH_2); 6.30 (m, 1H, *o*-tol); 6.46 (m, 1H, *o*-tol); 6.51 (m, 1H, *o*-tol); 7.20–7.40 (m, 16H, PPh_3 + *o*-tol). ^{31}P{^{1}H} NMR (202.46 MHz, CD_2Cl_2, r.t., ppm): δ = 27.6. ^{19}F NMR (470.55 MHz, CD_2Cl_2, r.t., ppm): −80.9 (t, $^4J_{FF}$ = 7 Hz, 3F, CF_3); −115.1, −115.9 (dq, $^2J_{FF}$ = 270 Hz, $^4J_{FF}$ = 9 Hz, 2F, C(O)CF_2); −126.0, −126.7 (d, $^2J_{FF}$ = 285 Hz, 2F, CF_2−CF_3). IR (KBr disk, cm^{-1}): $\tilde{\nu}$ = 3021 (m, C−H$_{aromat.}$); 2944 (m, C−H$_{aliphat.}$); 2226 (vs, C≡N); 1611 (vs, C=O); 1502 (vs, C=C); 1438 (m, P−C); 1230 (s, C−F). $C_{36}H_{30}N_2OF_7PNi$ (743.33): calcd. C 59.79, H 4.34, N 3.77; found C 59.4, H 4.4, N 4.0.

4.6. (SP-4-3)-[NiBr(2,4-xyl)(PPh$_3$)$_2$]

The synthesis was carried out as for (*SP*-4-3)-[NiBr(2-tol)(PPh$_3$)$_2$], except that 4.6 g (25 mmol) 2,4-dimethylbromobenzene was used yielding 8.6 g of a yellow solid (56%). ^{1}H NMR (200.13 MHz, $CDCl_3$, r.t., ppm): δ = 1.92 (s, 3H, *p*-CH_3), 2.02 (s, 3H, *o*-CH_3), 5.80 (s, 1H, *m*-CH xyl, between the methyl groups), 6.12 (d, 1H, *m*-CH xyl), 6.87 (d, 1H, *o*-CH xyl), 7.22 (m, 18H, PPh_3), 7.53 (m, 12H, PPh_3). ^{13}C{^{1}H} NMR (125.77 MHz, C_6D_6, r.t., ppm, not all carbons observed): δ = 20.7 (*p*-CH_3), 26.5 (*o*-CH_3), 125.0 (*m*-CH xyl), 130.0, 131.6, 132.0, 132.7 (d, $^2J_{CP}$ = 8.82 Hz), 144.0. ^{31}P{^{1}H} NMR (81.01 MHz, $CDCl_3$, r.t., ppm): δ = 22.5. IR (KBr disk, cm^{-1}): $\tilde{\nu}$ = 3048 (w, C−H$_{aromat.}$), 2914 (w, C−H$_{aliphat.}$), 1480 (m, C−C$_{aromat.}$), 1434, 1384, 1308 (s, C−H$_{aliphat.}$), 1093 (m, P−C), 741 (m, C−H$_{aromat.}$). MS (FAB+): *m*/*z* (fragment/relative intensity) = 582 ([M − o,o-xyl − Br]$^+$, 13), 367 ([o,o-xyl−PPh_3]$^+$, 50), 307 (13), 289 (12), 262 ([PPh_3]$^+$, 7), 154 (97), 136 (100), 105 ([o,o-xyl]$^+$, 23), 89 (81), 77 ([Ph]$^+$, 84), 63 (73), 51 (79). This compound was used without further purification.

4.7. (SP-4-3)-[Ni(**L¹**)(2,4-xyl)(PPh$_3$)] (**K¹″**)

3.37 g (4.38 mmol) (*SP*-4-3)-[NiBr(2,4-xyl)(PPh$_3$)$_2$] and 1.33 g (4.38 mmol) 4,4,5,5,6,6,6-heptafluoro-3-oxo-2-[pyrrolidin-(2Z)-ylidene]hexanenitrile (H**L¹**) were dissolved in toluene (150 mL). 7.9 mL (4.38 mmol) Sodiumbis(trimethylsilyl)amide (0.6 M in toluene) was added and the reaction mixture stirred overnight. After filtration over celite® the solvent was removed *in vacuo* and 150 mL methanol was added to the residue. After stirring overnight, the yellow precipitate was filtered, washed with methanol and dried *in vacuo* yielding 0.87 g of **K¹″** (27%). ^{1}H NMR (500.13 MHz, C_6D_6, r.t., ppm): δ = 0.82 (m, 2H, CH_2−CH_2−CH_2), 2.10 (s, 3H, *p*-CH_3), 2.36 (m, 2H, CH_2−CH_2−CH_2), 2.63 (s, 3H, *o*-CH_3), 2.69 (t, 2H, CH_2−CH_2−CH_2), 6.34 (s, 1H, *m*-CH xyl), 6.42 (s, 1H, *m*-CH xyl), 6.94 (m, 9H, PPh_3), 7.31 (s, 1H, *o*-CH xyl), 7.44 (m, 6H, PPh_3). ^{13}C{^{1}H} NMR (125.77 MHz, C_6D_6, r.t., ppm, not all carbons observed): δ = 20.0 (CH_2−CH_2−CH_2), 20.6 (*p*-CH_3), 25.5 (*o*-CH_3), 38.9 (CH_2−CH_2−CH_2), 63.6 (CH_2−CH_2−CH_2), 83.8 (C=C−CN), 125.0 and 129.9 (*m*-CH xyl), 130.3 (*m*-CH PPh_3), 130.4 (*p*-CH PPh_3), 134.5 (d, $^2J_{CP}$ = 10.1 Hz, *o*-CH PPh_3), 166.1 (C=O), 172.2 (C=C−CN). ^{31}P{^{1}H} NMR (202.46 MHz, C_6D_6, r.t., ppm): δ = 27.5. ^{19}F NMR (470.55 MHz, C_6D_6, r.t., ppm): δ = −80.98 (t, 3F, CF_3), −115.40 (q, 2F, C(O)CF_2), −125.79 (t, 2F, CF_2−CF_3). IR (KBr disk, cm^{-1}): $\tilde{\nu}$ = 3056 (w, C−H$_{aromat.}$), 2982 (w, C−H$_{aliphat.}$), 2214 (s, C≡N), 1591 (vs, C=O), 1516 (s, C−C$_{aromat.}$), 1434 (s, C−H$_{aliphat.}$), 1260, 1229, 1183 (s, C−F), 1114 (m, P−C), 750 (m, C−H$_{aromat.}$). MS (FAB+): *m*/*z* (fragment, relative intensity) = 730 ([M]$^{\bullet+}$, 1%), 729 ([M − H]$^+$, 2), 368 (31), 367 ([o,p-xyl−PPh_3]$^+$, 100), 307 (15), 289 (10), 263 ([$HPPh_3$]$^+$, 10), 262 ([PPh_3]$^+$, 8).

4.8. (SP-4-3)-[NiBr(2,6-xyl)(PPh$_3$)$_2$]

The synthesis was carried out as for (*SP*-4-3)-[NiBr(2-tol)(PPh$_3$)$_2$], except that 4.6 g (25 mmol) 2,6-dimethylbromobenzene was used yielding 7.9 g of a yellow solid (51%). ^{1}H NMR (200.13 MHz, $CDCl_3$, r.t., ppm): δ = 2.48 (s, 6H, CH_3), 5.96 (d, 2H, *m*-CH xyl), 6.28 (t, 1H, *p*-CH xyl), 7.28 (m, 15H, PPh_3), 7.55 (m, 13H, PPh_3), 7.75 (m, 2H, PPh_3). ^{13}C{^{1}H} NMR (125.77 MHz, C_6D_6, r.t., ppm, not all carbons observed):

δ = 26.8 (*o*-CH_3 xyl), 124.0 (*p*-CH xyl), 126.6 (*m*-CH xyl), 130.0, 131.9, 133.4, 143.2. $^{31}P\{^1H\}$ NMR (81.01 MHz, $CDCl_3$, r.t., ppm): δ = 21.5. IR (KBr disk, cm^{-1}): $\tilde{\nu}$ = 3140, 3051, 3002 (m, C–$H_{aromat.}$), 2984, 2952, 2900 (w, C–$H_{aliphat.}$), 1480 (m, C–$C_{aromat.}$), 1433, 1386, 1307 (vs, C–$H_{aliphat.}$), 1091 (s, P–C), 750, 740 (s, C–$H_{aromat.}$). MS (FAB+): *m*/*z* (fragment/relative intensity) = 582 ([M − o,o-xyl − Br]$^+$, 2), 367 ([o,o-xyl–PPh_3]$^+$, 3), 307 (10), 289 (9), 154 (90), 136 (100), 105 ([o,o-xyl]$^+$, 24), 89 (92), 77 ([Ph]$^+$, 96), 63 (86), 50 (92). This compound was used without further purification.

4.9. (SP-4-3)-[Ni(**L**^{1})(2,6-xyl)(PPh_3)] (**K**$^{1'''}$)

The synthesis was carried out as for **K**$^{1''}$ except that 2.92 g (4.00 mmol) (*SP*-4-3)-[NiBr(2,6-xyl)(PPh_3)$_2$], 1.22 g (4.00 mmol) H**L**^{1} and 7.2 mL (4.00 mmol) sodium bis(trimethylsilyl)amide were used, yielding 2.09 g of a yellow solid (72%). ^{1}H NMR (500.13 MHz, C_6D_6, r.t., ppm): δ = 0.82 (m, 2H, CH_2–CH_2–CH_2), 2.39 (m, 2H, CH_2–CH_2–CH_2), 2.58 (t, 2H, CH_2–CH_2–CH_2), 2.87 (s, 6H, *o*-CH_3), 6.42 (d, 2H, *m*-CH xyl), 6.70 (t, 1H, *p*-CH xyl), 6.92 (m, 9H, PPh_3), 7.38 (m, 6H, PPh_3). $^{13}C\{^1H\}$ NMR (125.77 MHz, C_6D_6, r.t., ppm, not all carbons observed): δ = 20.2 (CH_2–CH_2–CH_2), 25.9 (CH_3), 38.9 (CH_2–CH_2–CH_2), 63.3 (CH_2–CH_2–CH_2), 124.3 (*p*-CH xyl), 125.5 (*m*-CH xyl), 130.3 (d, $^3J_{CP}$ = 2.5 Hz, *m*-CH PPh_3), 130.7 (*p*-CH PPh_3), 134.3 (d, $^2J_{CP}$ = 10.1 Hz, *o*-CH PPh_3), 142.3 (d, $^3J_{CP}$ = 2.5 Hz, *o*-C xyl), 148.9 (d, $^2J_{CP}$ = 50.4 Hz, i-C xyl), 166.1 (C═O), 172.6 (C═C–CN). $^{31}P\{^1H\}$ NMR (202.46 MHz, C_6D_6, r.t., ppm): δ = 25.4. ^{19}F NMR (470.55 MHz, C_6D_6, r.t., ppm): δ = −81.00 (t, 3F, CF_3), −115.13 (m, 2F, C(O)CF_2), −125.51 (t, 2F, CF_2–CF_3). IR (KBr disk, cm^{-1}): $\tilde{\nu}$ = 3054 (w, C–$H_{aromat.}$), 2955, 2907 (w, C–$H_{aliphat.}$), 2214 (s, C≡N), 1586 (vs, C═O), 1512 (s, C–$C_{aromat.}$), 1435 (s, C–$H_{aliphat.}$), 1260, 1230, 1193 (vs, C–F), 1110 (s, P–C), 742 (m, C–$H_{aromat.}$). MS (EI): *m*/*z* (fragment, relative intensity) = 368 (26), 367 ([o,o-xyl–PPh_3]$^+$, 100), 263 ([$HPPh_3$]$^+$, 8), 262 ([PPh_3]$^+$, 34), 183 (28), 108 (7). MS (MALDI): *m*/*z* = 561 ([M − C_3F_7]$^+$), 508, 367 ([o,o-xyl–PPh_3]$^+$), 279, 263 ([$HPPh_3$]$^+$), 228. $C_{36}H_{30}F_7N_2OPNi$ (730.30): calcd. C 59.20, H 4.15, N 3.83; found C 59.0, H 4.2, N 3.8.

4.10. Decomposition experiments with 2-hexyne

The reaction of the complexes with 2-hexyne was carried out as previously described [15]. For GC/MS data of the reaction of **K**^{1} and **K**$^{1'}$ with 2-hexyne see Ref. [15].

4.10.1. Reaction of K$^{1''}$ with 2-hexyne

GC/MS: 4.8 min (7%, 2,4-dimethylphenol), 6.25 min (2%, β-hydride elimination product 3-(2,4-dimethylphenyl)-1,2-hexadiene), 6.32 min (2%, β-hydride elimination product 2-(2,4-dimethylphenyl)-2,3-hexadiene), 6.97 min (1%, rearrangement product 4,6-dimethyl-3-propyl-1*H*-indene), 12.3 min (45%, triphenylphosphane oxide).

2,4-Dimethylphenol

Retention time: 4.8 min; MS (EI): *m*/*z* (fragment, relative intensity) 122 ([M]$^{\bullet+}$, 97%), 121 ([M − H]$^+$, 51), 107 ([M − CH_3]$^+$, 100), 91 ([M − C_2H_7]$^+$, 19), 77 (Ph, 25).

3-(2,4-Dimethylphenyl)-1,2-hexadiene

Retention time: 6.25 min; MS (EI): *m*/*z* (fragment, relative intensity) 186 ([M]$^{\bullet+}$, 4%), 158 ([M − C_2H_4]$^{\bullet+}$, 11), 157 ([M − C_2H_5]$^+$, 19), 143 ([M − C_3H_7]$^+$, 100), 129 ([M − C_4H_9]$^+$, 18), 128 ([M − C_4H_{10}]$^{\bullet+}$, 52), 115 ([M − C_5H_{11}]$^+$, 15).

2-(2,4-Dimethylphenyl)-2,3-hexadiene

Retention time: 6.32 min; MS (EI): *m*/*z* (fragment, relative intensity) 186 ([M]$^{\bullet+}$, 2%), 171 ([M − CH_3]$^+$, 8), 158 ([M − C_2H_4]$^{\bullet+}$, 13), 157 ([M − C_2H_5]$^+$, 100), 143 ([M − C_3H_7]$^+$, 17), 142 ([M − C_3H_8]$^{\bullet+}$, 56), 129 ([M − C_4H_9]$^+$, 13), 128 ([M − C_4H_{10}]$^{\bullet+}$, 16), 115 ([M − C_5H_{11}]$^+$, 14).

4,6-Dimethyl-3-propyl-1H-indene

Retention time: 6.97 min; MS (EI): *m*/*z* (fragment, relative intensity) 186 ([M]$^{\bullet+}$, 100%), 171 ([M − CH_3]$^+$, 34), 157 ([M − C_2H_5]$^+$, 48), 143 ([M − C_3H_7]$^+$, 93), 142 ([M − C_3H_8]$^{\bullet+}$, 55), 129 ([M − C_4H_9]$^+$, 41), 128 ([M − C_4H_{10}]$^{\bullet+}$, 62), 115 ([M − C_5H_{11}]$^+$, 34).

4.11. Catalysis experiments with carbon monoxide and ethene

20 mg of the catalyst complex was dissolved in toluene (10 mL) in a 100 mL stainless steel autoclave with glass inlet under nitrogen atmosphere. Ethene (40 bar) and carbon monoxide (10 bar) were added and the reaction mixture was stirred for 24 h at 60 °C. The autoclave was weighed before and after adding the gases to determine the mass of the gases. If a solid precipitate formed this solid was separated, washed with methanol, dried *in vacuo* and characterised by IR spectroscopy.

4.12. Catalysis experiments with ethene

70 mg of the complex were dissolved in degassed and dried toluene (6 mL) in a stainless steel autoclave with glass inlet under nitrogen atmosphere and stirred for several days under a pressure of 70 bar of ethene. A GC/MS spectrum of the remaining solution was recorded.

4.12.1. **K**$^{1'}$/ethene only

Polyethylene yield 82%.

GC/MS: 3.0 min (26%, ethene oligomer $C_{10}H_{20}$), 3.1 min (18%, ethene oligomer $C_{10}H_{20}$ and 2-methylstyrene, signals are not properly separated), 3.2 min (7%, ethene oligomer $C_{10}H_{20}$), 4.0 min (1%, isomer of 1-(butenyl)-2-methylstyrene and ethene oligomer $C_{12}H_{24}$, signals are not properly separated), 4.3 min (4%, isomer of 1-(butenyl)-2-methylstyrene), 4.6 min (6%, ethene oligomer $C_{12}H_{24}$), 4.7 min (2%, isomer of 1-(butenyl)-2-methylstyrene and ethene oligomer $C_{12}H_{24}$, signals are not properly separated), 4.8 min (1%, ethene oligomer $C_{12}H_{24}$), 6.0 min (1%, ethene oligomer $C_{14}H_{18}$), 7.3 min (1%, ethene oligomer $C_{16}H_{32}$), 10.3 min (5%, triphenylphosphane).

4.12.2. **K**^{1}/ethene only

GC/MS (gaseous phase): 0.5 min (34%, ethene dimer/butene C_4H_8), 0.7 min (48%, ethene trimer/hexene C_6H_{12}), 1.9 min (2%, ethene tetramer/octene C_8H_{16}).

GC/MS (solution): 2.7 min (3%, ethene oligomer $C_{10}H_{20}$), 2.8 min (2%, ethene oligomer $C_{10}H_{20}$), 2.9 min (4%, ethene oligomer $C_{10}H_{20}$), 3.0 min (22%, ethene oligomer $C_{10}H_{20}$ and mesitylene, signals are not properly separated), 3.1 min (9%, ethene oligomer $C_{10}H_{20}$), 3.2 min (10%, ethene oligomer $C_{10}H_{20}$), 4.2 min (2%, ethene oligomer $C_{12}H_{24}$), 4.3 min (1%, ethene oligomer $C_{12}H_{24}$), 4.4 min (3%, ethene oligomer $C_{12}H_{24}$), 4.5 min (2%, ethene oligomer $C_{12}H_{24}$), 4.6 min (9%, ethene oligomer $C_{12}H_{24}$), 4.7 min (4%, ethene oligomer $C_{12}H_{24}$), 4.8 min (4%, ethene oligomer $C_{12}H_{24}$), 5.7 min (1%, ethene oligomer $C_{14}H_{28}$), 5.9 min (1%, ethene oligomer $C_{14}H_{28}$), 6.0 min (3%, ethene oligomer $C_{14}H_{18}$), 6.1 min (1%, isomer of 1-(butenyl)-2,4,6-trimethylbenzene and ethene oligomer $C_{14}H_{28}$, signals are not properly separated), 6.9, 7.0, 7.1 min (>1%, ethene oligomer $C_{16}H_{32}$), 7.2 min (2%, ethene oligomer $C_{16}H_{32}$), 8.0 min (>1%, *N*,*O*-ligand H**L**^{1}), 10.3 min (1%, triphenylphosphane).

4.12.3. **K**$^{2'}$/ethene only

GC/MS: 2.7 min (2%, ethene oligomer $C_{10}H_{20}$), 2.8 min (2%, ethene oligomer $C_{10}H_{20}$), 2.9 min (3%, ethene oligomer $C_{10}H_{20}$),

3.0 min (10%, ethene oligomer $C_{10}H_{20}$), 3.1 min (14%, ethene oligomer $C_{10}H_{20}$ and 2-methylstyrene, signals are not properly separated), 3.2 min (3%, ethene oligomer $C_{10}H_{20}$), 4.6 min (3%, ethene oligomer $C_{12}H_{24}$), 4.7 min (1%, ethene oligomer $C_{12}H_{24}$), 4.75 min (1%, ethene oligomer $C_{12}H_{24}$), 4.82 min (1%, isomer of 1-(butenyl)-2-methylstyrene), 6.0 min (2%, ethene oligomer $C_{14}H_{18}$), 7.2 min (1%, ethene oligomer $C_{16}H_{32}$), 10.3 min (1%, triphenylphosphane), 12.3 min (43%, triphenylphosphane oxide).

*4.12.4. **K**^{2}/ethene only*

GC/MS (gaseous phase): 0.5 min (17%, ethene dimer/butene C_4H_8), 0.7 min (23%, ethene trimer/hexene C_6H_{12}), 1.8 min (1%, ethene tetramer/octene C_8H_{16}).

GC/MS (solution): 2.7 min (6%, ethene oligomer $C_{10}H_{20}$), 2.8 min (4%, ethene oligomer $C_{10}H_{20}$), 2.9 min (11%, ethene oligomer $C_{10}H_{20}$), 3.0 min (17%, ethene oligomer $C_{10}H_{20}$ and mesitylene, signals are not properly separated), 3.1 min (11%, ethene oligomer $C_{10}H_{20}$), 4.3 min (1%, ethene oligomer $C_{12}H_{24}$), 4.4 min (0.5%, ethene oligomer $C_{12}H_{24}$), 4.5 min (3%, trimethylstyrol), 4.6 min (1%, ethene oligomer $C_{12}H_{24}$), 4.7 min (1%, ethene oligomer $C_{12}H_{24}$), 5.5 min (1%, isomer of 1-(butenyl)-2,4,6-trimethylbenzene), 5.8 min (7%, isomer of 1-(butenyl)-2,4,6-trimethylbenzene), 6.0 min (4%, isomer of 1-(butenyl)-2,4,6-trimethylbenzene), 7.0 min (0.5%, isomer of 1-(hexenyl)-2,4,6-trimethylbenzene), 7.2 min (0.5%, isomer of 1-(hexenyl)-2,4,6-trimethylbenzene), 8.7 min (5%, *N*,*O*-ligand H**L**^{2}), 10.3 min (10%, triphenylphosphane), 12.3 min (11%, triphenylphosphane oxide).

4.12.5. Mass spectra

4.12.5.1. 2,4,6-Trimethylstyrene. Retention time: 4.5 min; MS (EI): *m*/*z* (fragment, relative intensity) 146 ($[M]^{\bullet+}$, 100), 117 ($[M - H]^{+}$, 11), 131 ($[M - CH_3]^{+}$, 96), 129 (21), 128 (16), 116 (16), 115 (22), 91 ($[C_7H_7]^{+}$, 25).

4.12.5.2. Isomers of 1-(butenyl)-2,4,6-trimethylbenzene. Retention time: 5.5 min; MS (EI): *m*/*z* (fragment, relative intensity) 174 ($[M]^{\bullet+}$, 27), 173 ($[M - H]^{+}$, 12), 159 ($[M - CH_3]^{+}$, 100), 147 (61), 144 ($[M - 2CH_3]^{+}$, 30), 129 (17), 119 (15), 117 (13), 105 (9).

Retention time: 5.8 min; MS (EI): *m*/*z* (fragment, relative intensity) 174 ($[M]^{\bullet+}$, 62), 173 ($[M - H]^{+}$, 3), 159 ($[M - CH_3]^{+}$, 100), 144 ($[M - 2CH_3]^{+}$, 28), 131 (12), 129 (12), 128 (12), 119 (9), 117 (11), 105 (10).

Retention time: 6.0 min; MS (EI): *m*/*z* (fragment, relative intensity) 174 ($[M]^{\bullet+}$, 67), 173 ($[M - H]^{+}$, 2), 159 ($[M - CH_3]^{+}$, 100), 144 ($[M - 2CH_3]^{+}$, 25), 131 (13), 129 (14), 128 (13), 120 (14), 117 (12), 105 (11).

Acknowledgements

M.M.L. thanks the Studienstiftung des deutschen Volkes for a Ph.D. scholarship. We thank E. Hammes for technical assistance during X-ray data acquisition as well as Dr. P. Tommes and R. Bürgel for MS data.

Appendix A. Supplementary material

CCDC 802018 (**HL**^{1}), 802019 (**HL**^{2}), 802020 (**HL**^{3}), 802021 (**K**^{1}), 802022 (**K**^{2}) and 802023 (**K**^{3}) contain the supplementary crystallographic data for this paper. These data can be obtained free of charge from The Cambridge Crystallographic Data Centre via www.ccdc.cam.ac.uk/data_request/cif.

Appendix B. Supplementary material

Supplementary data related to this article can be found at http://dx.doi.org/10.1016/j.jorganchem.2012.08.030.

References

[1] A. Sommazzi, F. Garbassi, Prog. Polym. Sci. 22 (1997) 1547–1605.
[2] C. Bianchini, A. Meli, Coord. Chem. Rev. 225 (2002) 35–66.
[3] C.E. Ash, Int. J. Polym. Mater. 30 (1995) 1–13.
[4] R.G.W. Norrish, F.W. Kirkbride, J. Chem. Soc. (1932) 1518–1530.
[5] B.J. Lommerts, E.A. Klop, J. Aerts, J. Polym. Sci. B Polym. Phys. 31 (1993) 1319–1330.
[6] G.H. Hartley, J.E. Guillet, Macromolecules 1 (1968) 165–170.
[7] F.Y. Xu, J.C.W. Chien, Macromolecules 26 (1993) 3485–3489.
[8] E. Drent, Shell Internationale Research Maatschappij B.V., EP 121965, 1984.
[9] E. Drent, J.A.M. v. Broekhoven, M.J. Doyle, J. Organomet. Chem. 417 (1991) 235–251.
[10] E. Drent, M.C.T. de Kock, Shell Oil Company, US 5688909, 1997.
[11] E. Drent, P.H.M. Budzelaar, Chem. Rev. 96 (1996) 663–681.
[12] W. Kläui, J. Bongards, G.J. Reiß, Angew. Chem. Int. Ed. 39 (2000) 3894–3896.
[13] U. Beckmann, E. Eichberger, M. Lindner, M. Bongartz, P.C. Kunz, Eur. J. Org. Chem. 24 (2008) 4139–4147.
[14] U. Beckmann, G. Hägele, W. Frank, Eur. J. Inorg. Chem. (2010) 1670–1678.
[15] M.M. Lindner, U. Beckmann, E. Eichberger, G.J. Reiß, W. Kläui, Eur. J. Inorg. Chem. (2010) 2352–2360.
[16] U. Beckmann, E. Eichberger, A. Rufińska, R. Sablong, W. Kläui, J. Catal. 283 (2011) 143–148.
[17] H.E. Gottlieb, V. Kotlyar, A. Nudelman, J. Org. Chem. 62 (1997) 7512–7515.
[18] V. Wray, Annu. Rep. NMR Spectrosc. 10B (1980) 1.
[19] A. Klein, Z. Anorg. Allg. Chem. 627 (2001) 645–650.
[20] M.D. Raush, F.E. Tibbets, Inorg. Chem. 9 (1970) 512–516.
[21] K.P. MacKinnon, B.O. West, Aust. J. Chem. 21 (1968) 2801–2804.